

Finesse and sensitivity gain in cavity-enhanced absorption spectroscopy of biomolecules in solution

Timothy McGarvey, André Conjusteau and Hideo Mabuchi

Mail Code 266-33, California Institute of Technology, Pasadena, CA 91125

mgarvey@caltech.edu

Abstract: We describe a ‘wet mirror’ apparatus for cw cavity-enhanced absorption measurements with Bacteriochlorophyll *a* (BChla) in solution and show that it achieves the full sensitivity gain ($\approx 2.3 \times 10^4$) afforded by the finesse (3.4×10^4) and loss distribution of our optical resonator. This result provides an important proof-of-principle demonstration for solution-phase cavity-enhanced spectroscopy; straightforward extrapolation to a system with state-of-the-art low-loss mirrors and shot-noise-limited performance indicates that single molecule sensitivity in liquids is within reach of current technology. With the probe laser locked to the cavity resonance, our instrument achieves a sensitivity $\approx 3.4 \times 10^{-8}/\sqrt{\text{Hz}}$ (for a sample of length 1.75 mm) with 100 kHz bandwidth and can reliably detect sub-nM concentrations of BChla with 1 ms integration time.

© 2006 Optical Society of America

OCIS codes: (120.2230) Fabry-Perot; (300.6250) Condensed matter spectroscopy

References and links

1. R. E. Kunz, “Optimizing integrated optical chips for label-free (bio-)chemical sensing,” *Anal. Bioanal. Chem.* **384**, 180–190 (2006); N. Kinrot and M. Nathan, “Investigation of a Periodically-Segmented Waveguide Fabry-Pérot Interferometer for Use as a Chemical/Biosensor,” *J. Lightwave Technol.* **24**, 2139–2145 (2006).
2. A. J. Hallock, E. Berman and R. N. Zare, “Ultratrace Kinetic Measurements of the Reduction of Methylene Blue,” *J. Am. Chem. Soc.* **125**, 1158–1159 (2003).
3. J. Ye, L.-S. Ma and J. L. Hall, “Ultrasensitive detections in atomic and molecular physics: demonstration in molecular overtone spectroscopy,” *J. Opt. Soc. Am. B* **15**, 6–15 (1998).
4. A. C. R. Pipino, “Monolithic folded resonator for evanescent wave cavity ringdown spectroscopy,” *Appl. Opt.* **39**, 1449–1453 (2000).
5. J. L. Nadeau, V. S. Ilchenko, D. Kossokovski, G. H. Bearman and L. Maleki, “High-Q whispering-gallery mode sensor in liquids,” *Proc. SPIE* **4629**, 172–180 (2002).
6. L. van der Sneppen, A. Wiskerke, F. Ariese, C. Gooijer and W. Ubachs, “Improving the sensitivity of HPLC absorption detection by cavity ring-down spectroscopy in a liquid-only cavity” *Anal. Chim. Acta* **558**, 2–6 (2006).
7. S. Xu, G. Sha and J. Xie, “Cavity ring-down spectroscopy in the liquid phase,” *Rev. Sci. Instrum.* **73**, 255–258 (2002).
8. K. L. Bechtel, R. N. Zare, A. A. Kachanov, S. S. Sanders and B. A. Paldus, “Moving beyond Traditional UV-Visible Absorption Detection: Cavity Ring-Down Spectroscopy for HPLC,” *Anal. Chem.* **77**, 1177–1182 (2005).
9. S. E. Fiedler, A. Hese and A. A. Ruth, “Incoherent broad-band cavity-enhanced absorption spectroscopy of liquids,” *Rev. Sci. Instrum.* **76**, 023107 (2005).
10. M. E. Long, R. L. Swofford and A. C. Albrecht, “Thermal Lens Technique — New Method of Absorption Spectroscopy,” *Science* **191**, 183–185 (1976).
11. C. K. N. Patel and A. C. Tam, “Pulsed optoacoustic spectroscopy of condensed matter,” *Rev. Mod. Phys.* **53**, 517–550 (1981).
12. F. J. Blanco, M. Agirregabiria, J. Berganzo, K. Mayora, J. Elizalde, A. Calle, C. Dominguez and L. M. Lechuga, “Microfluidic-optical integrated CMOS compatible devices for label-free biochemical sensing,” *J. Micromech. Microeng.* **16**, 1006–1016 (2006).

13. I. Eichwurz, H. Stiel, K. Teuchner, D. Leupold, H. Scheer, Y. Salomon and A. Scherz, "Photophysical Consequences of Coupling Bacteriochlorophyll *a* with Serine and its Resulting Solubility in Water," *Photochem. Photobiol.* **72**, 204–209 (2000); J. S. Connolly, E. B. Samuel and A. F. Janzen, "Effects of solvent on the fluorescence properties of bacteriochlorophyll *a*," *Photochem. Photobiol.* **36**, 565–574 (1982).
14. M. Tokeshi, M. Uchida, A. Hibara, T. Sawada and T. Kitamori, "Determination of Subyctomole Amounts of Nonfluorescent Molecules Using a Thermal Lens Microscope: Subsingle-Molecule Determination," *Anal. Chem.* **73**, 2112–2116 (2001).
15. H. Mabuchi, J. Ye and H. J. Kimble, "Full observation of single-atom dynamics in cavity QED," *Appl. Phys. B* **68**, 1095–1108 (1999).
16. A. E. Siegman, *Lasers* (University Science Books, Sausalito, 1986).
17. G. Rempe, R. J. Thompson, H. J. Kimble and R. Lalezari, "Measurement of ultralow losses in an optical interferometer," *Opt. Lett.* **17**, 363–365 (1992).
18. A. M. van Oijen, M. Ketelaars, J. Köhler, T. J. Aartsma and J. Schmidt, "Spectroscopy of Individual Light-Harvesting 2 Complexes of *Rhodospseudomonas acidophila*: Diagonal Disorder, Intercomplex Heterogeneity, Spectral Diffusion, and Energy Transfer in the B800 Band," *Biophys. J.* **78**, 1570–1577 (2000).
19. H. A. Schuessler, S. H. Chen, Z. Rong, Z. C. Tang and E. C. Benck, "Cavity-enhanced photothermal spectroscopy: dynamics, sensitivity and spatial resolution," *Appl. Opt.* **31**, 2669–2677 (1992).
20. E. D. Black, I. S. Grudinin, S. R. Rao and K. G. Libbrecht, "Enhanced photothermal displacement spectroscopy for thin-film characterization using a Fabry-Perot resonator," *J. Appl. Phys.* **95**, 7655–7659 (2004).

1. Introduction

Efforts to improve the sensitivity of solution-phase optical absorption spectroscopy are motivated by applications in label-free biosensing [1] and in the characterization of low-concentration chemical reaction kinetics [2]. Approaches based on the use of high-finesse optical resonators are motivated by results achieved in analogous gas-phase experiments—experiments involving vibrational overtones of gas-phase molecules [3] have achieved detection thresholds as low as $1.5 \times 10^{-13}/\sqrt{\text{Hz}}$. For largely technical reasons, it has proven quite difficult for experiments on molecules in solution to approach such levels of sensitivity.

Here we present a significant technical advance in cw solution-phase optical absorption spectroscopy, in which we demonstrate that it is possible in practice to realize the full sensitivity gain that is made available via incorporation of a high-finesse Fabry-Perot cavity. In gas-phase experiments one can effectively take such finesse-limited sensitivity gains for granted, but the introduction of liquids into the intracavity volume can substantially complicate the requirements for performing reliable optical absorption measurements. In our scenario with a Fabry-Perot resonator, *e.g.*, mechanical and thermal stability of the cavity are substantially compromised by the presence of liquid between the mirrors. Mechanical couplings and hydrodynamic phenomena associated with sample injection likewise introduce various difficulties that would not arise in an analogous gas-phase experiment. Setups based on evanescent-wave coupling to light circulating in a dielectric resonator [4, 5] are less vulnerable to such effects, but would seem to have an ultimate sensitivity disadvantage as the molecules of interest can access only a weak tail of the optical mode function.

Our experiment incorporates a short ($l = 1.75$ mm) high-finesse ($F_0 \approx 5 \times 10^4$ when empty) Fabry-Perot resonator that is entirely filled with liquid sample, such that the mirror surfaces are in direct contact with fluid. This type of 'wet mirror' configuration (which is similar to that of Van der Sneppen *et al.* [6]) allows us to avoid the presence of optically-lossy surfaces within the cavity, and preserves the full finesse afforded by mirror losses provided the solvent itself has sufficiently low absorption. In the work described here we chose to test our instrument's performance with ultra-dilute samples of Bacteriochlorophyll *a* (BChla) dissolved in d_6 -acetone. We achieve an optical absorption sensitivity of $\approx 3.4 \times 10^{-8}/\sqrt{\text{Hz}}$ and find that with 1 ms integration time we are able reliably to measure BChla concentrations as low as ~ 200 pM. In comparison with other high-sensitivity optical absorption techniques that have been applied to liquid samples, such as cavity ring-down [7, 8, 6], incoherent broad-band cavity-enhanced

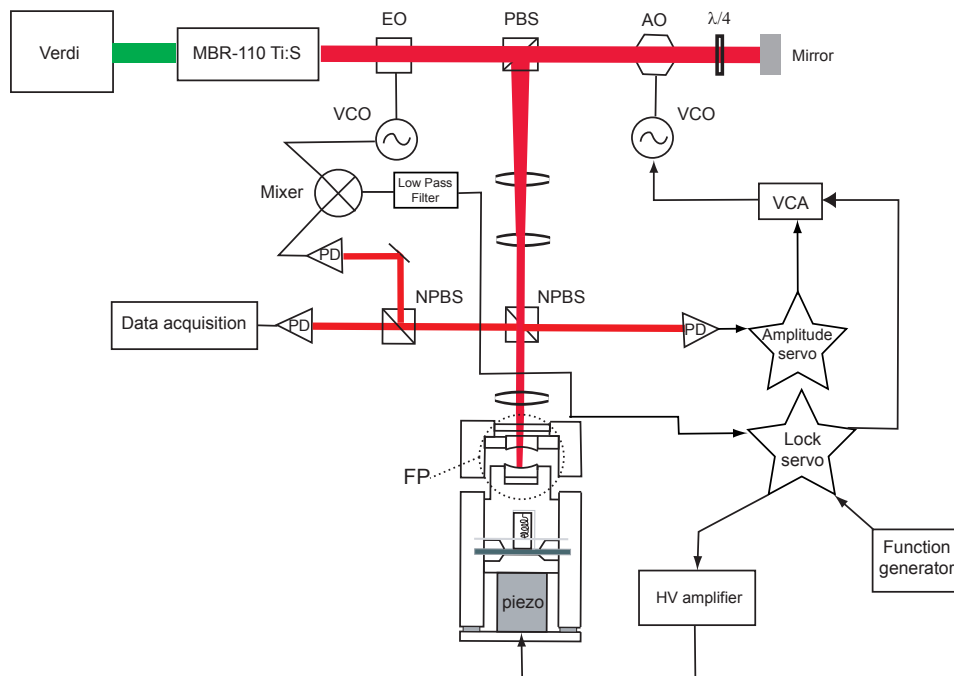


Fig. 1. Schematic diagram of the experimental setup. PBS: polarizing beam-splitter; NBPS: non-polarizing beam-splitter; $\lambda/4$: quarter-wave plate; HV: high voltage. See text for other designations.

absorption [9], thermal lens effect [10] and photo-acoustic [11] spectroscopy, we note that our approach achieves comparable (and is capable of better) sensitivity while requiring only small amounts of sample (several ml). In its current configuration, which exhibits a fair amount of excess technical noise, our setup has an absorption detection threshold $\approx 7 \times 10^{-6} \text{ cm}^{-1}$ with 1 ms integration time; further improvements to the laser and cavity stabilization would make it possible to approach a shot-noise-limited value $\approx 3.5 \times 10^{-8} \text{ cm}^{-1}$ (the works cited above report detection thresholds in the range $\sim 10^{-5} - -10^{-7} \text{ cm}^{-1}$).

Setting aside absolute sensitivity, however, we consider the main result of this paper to be the quantitative analysis that matches our observed sensitivity gain ($\approx 2.3 \times 10^4$ relative to single-pass absorption) with theoretical predictions based on our cavity finesse 3.4×10^4 and internal losses. We believe that this agreement provides a proof of concept such that we may reasonably extrapolate a prediction of the performance that could be achieved with state-of-the-art low-loss mirrors and shot-noise-limited readout. In this way we find that sensitivities approaching $10^{-12}/\sqrt{\text{Hz}}$ could be achievable, which would make room temperature, liquid-phase single-BChla-molecule absorption spectroscopy a real possibility (see Discussion). Such a setup would require a very short ($l \sim 10 \mu\text{m}$) cavity in order to suppress solvent-induced losses; this dimension emphasizes the possibility of integration with microfluidic sample delivery [12].

2. Apparatus

A schematic of our setup is shown in Figure 1. The BChla-doped d_6 -acetone sample is injected into the intracavity volume of a hermetically-sealed Fabry-Perot (FP) resonator (see below). A Verdi-pumped MBR-110 Titanium Sapphire laser (Ti:S) provides laser light at 783nm (cor-

responding to the Q_y transition in BChla, with expected extinction coefficient $\approx 6 \times 10^4 \text{ M}^{-1} \text{ cm}^{-1}$ in acetone [13]; the Q_y peak sits at 770nm but our Ti:S did not operate stably there with the mirror set we have) for probing the cavity response. The Ti:S laser is pre-stabilized to an internal reference cavity and an acousto-optic modulator (AO) driven by a voltage-controlled oscillator (VCO) is utilized to produce a frequency-shifted beam that can be locked to the FP (with 100 kHz bandwidth). The error signal for the latter servo is derived by the usual demodulation of frequency modulation (FM) sidebands produced by an electro-optic modulator (EO). We additionally apply integral feedback to a piezo-electric actuator of the FP cavity length in order to compensate for slow drift. Some intensity stabilization is implemented via feedback to a variable-gain amplifier (VGA) on the rf input of the VCO driving the AO.

The beam reflected from the FP cavity is split and directed to two different photodetectors (PD): one for measuring and recording the time-dependent reflectivity and one for generating the FM error signal. Note that we used a rather weak probe beam (incident power $6 \times 10^{-8} \text{ W}$, essentially the lowest at which we could stay locked to the cavity) in order to avoid potential nonlinearities; we therefore utilized avalanche photodiodes (APD's) for both purposes (a Menlo Systems APD-210 for the error signal and a Hamamatsu C5460-01 for the data acquisition, neither of which operate in Geiger mode). The analog bandwidth of the data acquisition photodetector was 100 kHz and we digitized at 1 MHz sampling rate at 14 bit resolution.

The FP mirrors were fabricated by Research Electro-Optics (Boulder, Colorado), with specified loss $< 20 \text{ ppm}$ (in air) at a center wavelength of 770nm for the high-reflectivity coating run. The super-polished substrates had 10 cm radius of curvature. The mechanical assembly of the FP incorporates a solvent-tight glass window to allow optical access to one side of the cavity (fixed mirror), but the scanning-mirror side is sealed by a flexible sheet of (opaque) Kalrez; the piezo-actuator pushes the scanning mirror mount through the flexible Kalrez sheet. This construction allowed us to ensure that no solvent could reach the associated electrical components, but limited us to making optical reflection (as opposed to transmission) measurements for detecting intracavity absorption. A clean 'plumbing' system was integrated with the FP assembly so that solution could be pulled up through the cavity by applying suction from above (this proved to be the best technique for filling the cavity with bubble-free liquid sample). Great care had to be taken to ensure mechanical stability of the entire assembly and to suppress control vibrational coupling from the plumbing components. Also, since the solvent we employed (d_6 -acetone) to carry the BChla molecules is sufficiently transparent only before prolonged exposure to air, we found it necessary to purge the cavity with dry nitrogen before each experiment.

3. Cavity-enhanced absorption measurements

Our discussion here will focus on characterizing the expected sensitivity gain in cavity-enhanced absorption measurements, with an implicit assumption that what one wants to achieve is the ability to measure absorption caused by a small number of molecules with as high a bandwidth as possible (which is quite different than in methods that achieve high sensitivity with long averaging times, such as [14]). Ultimately, we hope that cavity-enhanced spectroscopy with ultra-high finesse can enable single molecule studies in which one continuously monitors the absorption of a non-fluorescing, wild-type molecule at one or more optical wavelengths to detect reactions or conformational changes in real time (as can already be done with strongly absorbing gas-phase alkali atoms [15]). Towards that end, the current study is mainly intended to demonstrate that high-finesse cavities can indeed be utilized for liquid-phase absorption spectroscopy, provided great care is taken to suppress background losses associated with solvent and sample containment.

3.1. Absorption estimators and the operational sensitivity gain

Consider a single-pass measurement of absorption in a sample of length l . We assume that the sample consists of dopant molecules suspended in a solvent, and that it is possible to make measurements of either plain solvent or doped solvent under otherwise identical conditions. If the power absorption coefficient of the substance of interest is α , and the solvent/sample-holder contribute background loss $e^{-\delta}$, we have a total transmitted power

$$P_{\text{sp-}} = P_{\text{inc}} e^{-\delta} \quad (1)$$

with undoped solvent and

$$P_{\text{sp+}} = P_{\text{inc}} e^{-\delta} e^{-\alpha l} \quad (2)$$

with doped solvent. It is straightforward to estimate αl from measurements of $P_{\text{sp-}}$ and $P_{\text{sp+}}$:

$$(\alpha l)_{\text{sp}} = \ln [P_{\text{sp-}}] - \ln [P_{\text{sp+}}]. \quad (3)$$

The sensitivity of $(\alpha l)_{\text{sp}}$ to uncertainties in the measured optical powers is easy to compute:

$$\Delta(\alpha l)_{\text{sp}} = \left\{ \frac{\partial (\alpha l)_{\text{sp}}}{\partial P_{\text{sp-}}} \right\} \Delta P_{\text{sp-}} + \left\{ \frac{\partial (\alpha l)_{\text{sp}}}{\partial P_{\text{sp+}}} \right\} \Delta P_{\text{sp+}} \quad (4)$$

$$= \frac{\Delta P_{\text{sp-}}}{P_{\text{sp-}}} - \frac{\Delta P_{\text{sp+}}}{P_{\text{sp+}}}. \quad (5)$$

We thus see that the fractional uncertainties in $P_{\text{sp-}}$ and $P_{\text{sp+}}$ translate directly into absolute uncertainties in $(\alpha l)_{\text{sp}}$. Hence, for very small absorption, the detection threshold for single-pass measurement is equal to the fractional uncertainty of the optical power measurements. The aim of cavity-enhanced absorption is to improve upon this, *i.e.*, to obtain a (much) lower detection threshold for the same sample length l and fractional uncertainty in measuring optical power.

Here we consider cavity-enhanced absorption measurements performed via detection of reflected optical power from a cavity of length l , filled with the liquid sample. (The reason for considering reflection rather than transmission measurements has to do with the way we chose to construct a cavity whose length can be controlled by a piezo-actuator and yet is completely leak-tight.) The reflected power is [16]

$$P_{\text{ce-}} = P_{\text{inc}} \frac{(r_1^2 - g_{\text{rt-}})^2}{r_1^2 (1 - g_{\text{rt-}})^2}, \quad g_{\text{rt-}} = r_1 r_2 e^{-\delta/2} \quad (6)$$

with undoped solvent and

$$P_{\text{ce+}} = P_{\text{inc}} \frac{(r_1^2 - g_{\text{rt+}})^2}{r_1^2 (1 - g_{\text{rt+}})^2}, \quad g_{\text{rt+}} = r_1 r_2 e^{-\delta/2} e^{-\alpha l} = g_{\text{rt-}} e^{-\alpha l} \quad (7)$$

with doped solvent. Here $r_1 = \sqrt{1 - t_1^2}$ and $r_2 = \sqrt{1 - t_2^2}$, where t_1^2 and t_2^2 are the power transmission coefficients of the first and second cavity mirror (we assume we are reflecting off of the first mirror), and δ includes background power losses from both the solvent and the mirror coatings. Note that the equation relating $P_{\text{ce+}}$ and αl contains three other parameters, $\{P_{\text{inc}}, r_1, g_{\text{rt-}}\}$. It is thus necessary to measure at least three additional quantities to form an estimator. In cavity-reflection measurements the most natural set is $\{P_{\text{inc}}, P_{\text{ce-}}, F_{-}\}$, where F_{-}

is the cavity finesse with undoped solvent (see below). Tedious but straightforward calculations then yield a corresponding cavity-enhanced absorption estimator:

$$(\alpha l)_{ce} = \ln \left[\frac{1 - \frac{\pi}{2F_-}}{1 + \frac{\pi}{2F_-} R_-} \right] + \ln \left[\frac{Q + \frac{\pi}{2F_-} R_+}{Q - \frac{\pi}{2F_-}} \right], \quad (8)$$

where

$$R_- \equiv \sqrt{\frac{P_{ce-}}{P_{inc}}}, \quad R_+ \equiv \sqrt{\frac{P_{ce+}}{P_{inc}}}, \quad Q \equiv \frac{1 - R_+}{1 - R_-}. \quad (9)$$

For $\alpha l \ll 1$ and to leading order in $\pi/2F_-$ this can be approximated by

$$(\alpha l)_{ce\approx} = \frac{\pi}{F_-} \left(\frac{R_+ - R_-}{1 - R_+} \right) = \frac{\pi}{F_-} \left(\frac{\sqrt{P_{ce+}} - \sqrt{P_{ce-}}}{\sqrt{P_{inc}} - \sqrt{P_{ce+}}} \right). \quad (10)$$

If we want to account for a mode-matching efficiency $\varepsilon < 1$, we can set

$$P_{inc} \rightarrow \varepsilon P_{inc}, \quad P_{ce-} \rightarrow P_{rfl-} - (1 - \varepsilon) P_{inc}, \quad P_{ce+} \rightarrow P_{rfl+} - (1 - \varepsilon) P_{inc}, \quad (11)$$

$$R_- \rightarrow \sqrt{\frac{P_{rfl-} - (1 - \varepsilon) P_{inc}}{\varepsilon P_{inc}}} \equiv R_{-\varepsilon}, \quad R_+ \rightarrow \sqrt{\frac{P_{rfl+} - (1 - \varepsilon) P_{inc}}{\varepsilon P_{inc}}} \equiv R_{+\varepsilon}, \quad (12)$$

where $P_{rfl\pm}$ represent the total power measured in reflection from the cavity with undoped and doped solvent. So then

$$(\alpha l)_{ce\approx} \rightarrow \frac{\pi}{F_-} \left(\frac{\sqrt{P_{rfl+} - (1 - \varepsilon) P_{inc}} - \sqrt{P_{rfl-} - (1 - \varepsilon) P_{inc}}}{\sqrt{\varepsilon P_{inc}} - \sqrt{P_{rfl+} - (1 - \varepsilon) P_{inc}}} \right), \quad (13)$$

and similarly for the exact $(\alpha l)_{ce}$.

Returning now to the case $\varepsilon = 1$ for simplicity, we note that

$$\frac{\partial (\alpha l)_{ce\approx}}{\partial P_{ce+}} = \frac{\pi}{2F_-} \frac{\sqrt{P_{inc}} - \sqrt{P_{ce-}}}{\sqrt{P_{ce+}} (\sqrt{P_{inc}} - \sqrt{P_{ce+}})^2}, \quad (14)$$

$$\left| \frac{\partial (\alpha l)_{ce\approx}}{\partial P_{ce+}} \right| \Delta P_{ce+} = \frac{\pi}{2F_-} \frac{1 - R_-}{1 - R_+} \frac{R_+}{1 - R_+} \left(\frac{\Delta P_{ce+}}{P_{ce+}} \right). \quad (15)$$

From the latter expression we may thus define an ‘uncertainty suppression factor’ $U_{ce\approx}$:

$$\left| \frac{\partial (\alpha l)_{ce\approx}}{\partial P_{ce+}} \right| \Delta P_{ce+} = U_{ce\approx}^{-1} \left(\frac{\Delta P_{ce+}}{P_{ce+}} \right). \quad (16)$$

Since we saw above that the corresponding uncertainty suppression factor of single-pass measurement is $U_{sp} = -1$, we conclude that the operational sensitivity gain of cavity-enhanced absorption relative to single-pass is

$$G_{op} \equiv \left| \frac{U_{ce\approx}}{U_{sp}} \right| = U_{ce\approx} = \left(\frac{\pi}{2F_-} \frac{1 - R_-}{1 - R_+} \frac{R_+}{1 - R_+} \right)^{-1}. \quad (17)$$

Recall that this expression assumes $\{\alpha l, \pi/2F_-\} \ll 1$. Next we will try to estimate the magnitude of G_{op} under realistic assumptions on the cavity parameters.

Under the mild condition $\{R_-, R_+\} < 1/2$, which implies $r_1 \approx r_2$ and $\delta + \alpha l \lesssim t_{1,2}^2$, we have

$$\frac{1 - R_-}{1 - R_+} \frac{R_+}{1 - R_+} < 2, \quad (18)$$

in which case the contribution of ΔP_{ce+} to $\Delta(\alpha l)_{ce\approx}$ is bounded by

$$\left| \frac{\partial(\alpha l)_{ce\approx}}{\partial P_{ce+}} \right| \Delta P_{ce+} < \frac{\pi}{F_-} \left(\frac{\Delta P_{ce+}}{P_{ce+}} \right). \quad (19)$$

Indeed, if $\alpha l \ll 1$ then $R_- \approx R_+$ and we can solve for the condition $U_{ce\approx} > F_-$, which requires

$$\frac{\pi}{2} \frac{1-R_-}{1-R_+} \frac{R_+}{1-R_+} \approx \frac{\pi}{2} \frac{R_+}{1-R_+} < 1, \quad (20)$$

hence $R_+ \lesssim 0.4$. Under this condition (which is still relatively mild, being satisfied, *e.g.*, by $\delta = t_1^2 = t_2^2$ and $\alpha l \ll \delta$) we achieve a suppression $\gtrsim F_-$ in the effect of a fractional uncertainty in power measurement on our ability to estimate αl . Compared to the single-pass method, our detection threshold is thus smaller (better) by a factor of order F_-^{-1} for the same sample length l and fractional power uncertainty.

For completeness we include

$$\left| \frac{\partial(\alpha l)_{ce\approx}}{\partial F_-} \right| \Delta F_- = \frac{\pi}{F_-} \frac{R_- - R_+}{1 - R_+} \left(\frac{\Delta F_-}{F_-} \right), \quad (21)$$

$$\left| \frac{\partial(\alpha l)_{ce\approx}}{\partial P_{inc}} \right| \Delta P_{inc} = \frac{\pi}{2F_-} \frac{R_- - R_+}{1 - R_+} \frac{1}{1 - R_+} \left(\frac{\Delta P_{inc}}{P_{inc}} \right), \quad (22)$$

$$\left| \frac{\partial(\alpha l)_{ce\approx}}{\partial P_{ce-}} \right| \Delta P_{ce-} = \frac{\pi}{2F_-} \frac{R_-}{1 - R_+} \left(\frac{\Delta P_{ce-}}{P_{ce-}} \right), \quad (23)$$

all of which have uncertainty suppression factors comparable to (in the case of P_{ce-}) or better (in the case of F_- and P_{inc}) than that for P_{ce+} considered above. The corresponding expressions are much more cumbersome, though still calculable, in case of $\varepsilon < 1$. For P_{ce+} , for example,

$$\left| \frac{\partial(\alpha l)_{cav}}{\partial P_{tr+}} \right| \Delta P_{tr+} = \frac{\pi}{2F_-} \frac{1 - R_{-\varepsilon}}{1 - R_{+\varepsilon}} \frac{R_{+\varepsilon}}{1 - R_{+\varepsilon}} \left(\frac{\Delta P_{tr+}}{P_{tr+} - (1 - \varepsilon)P_{inc}} \right), \quad (24)$$

where $R_{\pm\varepsilon}$ are as defined in Eq. (12).

Note that in general we may assume F_- and ε to be fixed parameters. As a result, any uncertainty about them will result in a corresponding ‘calibration’ uncertainty in cavity-enhanced measurement of αl . However, long as P_{inc} can be held constant (presumably by some sort of active servo-control) and P_{ce-} is well known (by virtue of long integration time in a ‘set-up’ phase of the experiment), it follows that ΔP_{ce+} will determine the overall measurement uncertainty. Ultimately one could hope to reach the shot-noise limited value,

$$\frac{\Delta P_{ce+}}{P_{ce+}} \rightarrow \frac{\sqrt{(S/q)P_{ce+}\tau}}{(S/q)P_{ce+}\tau} = \frac{1}{\sqrt{(S/q)P_{ce+}\tau}}, \quad (25)$$

$$\Rightarrow \left| \frac{\partial(\alpha l)_{ce\approx}}{\partial P_{ce+}} \right| \Delta P_{ce+} \rightarrow \frac{U_{ce\approx}^{-1}}{\sqrt{(S/q)P_{ce+}\tau}}. \quad (26)$$

Here S is the photodetection sensitivity (in units of A/W), q is the electron charge and τ is the integration time. Note that (S/q) is bounded above by the inverse photon energy $(\hbar\omega)^{-1}$.

3.2. Theoretical sensitivity gain

Given a fractional uncertainty η in measuring optical power, we have

$$\Delta(\alpha l)_{ce} = \left(\frac{\partial(\alpha l)_{ce}}{\partial P_{ce+}} \right) \Delta P_{ce+} \rightarrow \left(\frac{\partial(\alpha l)_{ce}}{\partial P_{ce+}} \right) \eta P_{ce+}, \quad (27)$$

$$\Delta(\alpha l)_{sp} = \left(\frac{\partial(\alpha l)_{sp}}{\partial P_{sp+}} \right) \Delta P_{sp+} \rightarrow \left(\frac{\partial(\alpha l)_{sp}}{\partial P_{sp+}} \right) \eta P_{sp+}. \quad (28)$$

We can thus define a theoretical uncertainty suppression factor for each method,

$$U_{\text{th:ce}} = \left(P_{\text{ce}+} \frac{\partial(\alpha l)_{\text{ce}}}{\partial P_{\text{ce}+}} \right)^{-1} = \frac{1}{l P_{\text{ce}+}} \left(\frac{\partial P_{\text{ce}+}}{\partial \alpha} \right)_{P_{\text{ce}+}}, \quad (29)$$

$$U_{\text{th:sp}} = \left(P_{\text{sp}+} \frac{\partial(\alpha l)_{\text{sp}}}{\partial P_{\text{sp}+}} \right)^{-1} = \frac{1}{l P_{\text{sp}+}} \left(\frac{\partial P_{\text{sp}+}}{\partial \alpha} \right)_{P_{\text{sp}+}}. \quad (30)$$

Using results from above we have $U_{\text{th:sp}} = -1$; for comparison with $U_{\text{ce}\infty}$, which we derived above from the form of the practical estimator, we will next compute $U_{\text{th:ce}}$ by a more direct route. Using

$$P_{\text{ce}+} = P_{\text{inc}} \frac{(r_1^2 - g_{\text{rt}+})^2}{r_1^2 (1 - g_{\text{rt}+})^2}, \quad (31)$$

we can compute

$$\frac{\partial P_{\text{ce}+}}{\partial \alpha} = 2l P_{\text{inc}} \frac{g_{\text{rt}+} (r_1^2 - g_{\text{rt}+}) (1 - r_1^2)}{r_1^2 (1 - g_{\text{rt}+})^3}, \quad (32)$$

$$\left(\frac{\partial P_{\text{ce}+}}{\partial \alpha} \right)_{P_{\text{ce}+}} = 2l P_{\text{ce}+} \frac{g_{\text{rt}+} (1 - r_1^2)}{(1 - g_{\text{rt}+}) (r_1^2 - g_{\text{rt}+})} \quad (33)$$

$$\implies U_{\text{th:ce}} = 2 \frac{g_{\text{rt}+} (1 - r_1^2)}{(1 - g_{\text{rt}+}) (r_1^2 - g_{\text{rt}+})}. \quad (34)$$

It follows that the theoretical sensitivity gain is

$$G_{\text{th}} \equiv \frac{U_{\text{th:ce}}}{U_{\text{th:sp}}} = -2 \frac{g_{\text{rt}+} (1 - r_1^2)}{(1 - g_{\text{rt}+}) (r_1^2 - g_{\text{rt}+})}, \quad (35)$$

and it can be verified numerically that $G_{\text{th}} \approx G_{\text{op}}$ over an appropriate parameter range. The theoretical expression is useful for design purposes, whereas G_{op} is more useful in evaluating the performance of laboratory devices since it can be computed from directly measurable quantities only.

Note that $U_{\text{th:ce}}$ can be used to provide a theoretical expression (analogous to the operational version, Eq. (26)) for the minimum measurable absorption:

$$\Delta(\alpha l)_{\text{th:ce}} \geq \frac{U_{\text{th:ce}}^{-1}}{\sqrt{(S/q) P_{\text{ce}+} \tau}} \quad (36)$$

$$\rightarrow 2 \frac{(1 - g_{\text{rt}-}) (r_1^2 - g_{\text{rt}-})}{g_{\text{rt}-} (1 - r_1^2) \sqrt{(P_{\text{ce}-} \tau) / (\hbar \omega)}}. \quad (37)$$

Here we have taken $\alpha l \rightarrow 0$ and set $S/q \rightarrow (\hbar \omega)^{-1}$ as discussed above. (Note that this expression should not be used if one wants to make the physically unrealistic assumption $P_{\text{ce}-} \rightarrow 0$; to understand detection sensitivity in that limit one would need to analyze Poisson photon counting statistics.) Numerical sampling of function (37) suggests that optimization of $U_{\text{th:ce}}^{-1}$ mainly requires keeping δ as small as possible and depends only weakly on F_- (as long as it is reasonably high). However, unless the mirror transmissions are of the same order of magnitude as δ , the reflected power $P_{\text{ce}-}$ is a small fraction of P_{inc} and one does not bring down the shot-noise factor efficiently (relative, *e.g.*, to the intracavity circulating power seen by the molecules). Hence what seems best overall is F_- as high as possible with $\delta \approx \{t_1^2, t_2^2\}$, which leads as mentioned in the previous section to an overall uncertainty suppression on the order of F_-^{-1} .

3.3. Determination of finesse and mode-matching efficiency

Above we have presented several equations that account for the effects of imperfect mode-matching efficiency $\varepsilon < 1$. In practice it can be difficult to determine ε accurately, especially if one cavity mirror is physically inaccessible as in our hermetically sealed setup. Our approach was to match absorption estimates obtained at high BChla concentrations from the reflection dip, via Eq. (13), with estimates from the change in finesse, via Eq. (41) below (which does not depend on ε). At relatively high BChla concentrations (such that $\alpha l \gtrsim 2\pi/F_-$) both methods are reliable, whereas at low concentrations only the reflection dip yields precise measurements because the change-in-finesse approach is limited by laser/cavity jitter and nonlinearity of the piezo-actuator. Since ε is fixed by laser alignment, a determination from high-concentration measurements should remain valid for any αl .

The cavity finesse with doped or undoped solvent, F_{\pm} , can be experimentally determined by directly measuring both the axial spacing of TEM₀₀ modes, \mathcal{F} , and the cavity line-width, Δf_{\pm} , as $F_{\pm} = \mathcal{F}/\Delta f_{\pm}$. It can likewise be related directly to the total round-trip power loss [16], L_{\pm} , via $F_{\pm} = 2\pi/L_{\pm}$. The total losses can in turn be written as

$$L_- = 1 - g_{\text{rt}-}^2 \approx (1 - r_1^2) + (1 - r_2^2) + \delta, \quad (38)$$

$$L_+ = 1 - g_{\text{rt}+}^2 \approx (1 - r_1^2) + (1 - r_2^2) + \delta + 2\alpha l. \quad (39)$$

Assuming the mirror and solvent losses are independent of the concentration of BChla, the resonance widths Δf_{\pm} can be measured in the presence and absence of a given concentration of BChla to directly determine the loss it induces:

$$\frac{2\pi}{F_+} - \frac{2\pi}{F_-} = \frac{2\pi}{\mathcal{F}} (\Delta f_+ - \Delta f_-) = 2\alpha l, \quad (40)$$

so

$$(\alpha l)_{\Delta f} = \frac{\pi}{\mathcal{F}} (\Delta f_+ - \Delta f_-). \quad (41)$$

This estimator for the induced absorption does not depend on the TEM₀₀ mode-matching efficiency, and may thus be used to calibrate ε in a reflection-dip measurement taken at the same concentration of BChla. Explicitly, we equate expression (13) for $(\alpha l)_{\text{ce}\approx}$ to the measured value of $(\alpha l)_{\Delta f}$ and solve for ε in terms of the measured quantities F_- , P_{inc} , $P_{\text{ce}-}$ and $P_{\text{ce}+}$.

4. Data Summary

Data demonstrating the sensitivity of our device for measuring BChla absorption are summarized in Fig. 2. Our baseline measurements with undoped solvent gave $R_- = 0.48$ and we also measured (coincidentally) $\varepsilon = 0.48$. Various concentrations of Bchla (determined as series dilutions) were injected into a locked cavity and the intracavity losses due to Bchla absorption were measured by the reflection-dip method described in the previous section. We plot $(\alpha l)_{\text{ce}\approx}$ as a function of nominal BChla concentration, where each point and error bar represent the mean and uncertainty in the mean of three measurements (1 ms integration time). An extrapolation from a linear fit to high-concentration single-pass measurements $(\alpha l)_{\text{sp}}$ is also drawn in order to confirm the accuracy of our cavity-enhanced measurements. The extinction coefficient inferred from the latter measurements was $\approx 4.4 \times 10^4 \text{ M}^{-1} \text{ cm}^{-1}$, which is somewhat lower than the value of $\approx 6 \times 10^4$ (at 783 nm) that has been determined in more careful measurements [13]; we interpret this discrepancy to be an indication that the actual BChla concentration in our samples was somewhat lower than we assumed on the basis of the dopant/solvent ratio (the manufacturer designated the substance we used as ‘partially purified’ BChla).

Aside from the linear behavior at high concentrations, the salient feature of our data plot is the flattening at low concentrations. The flattening occurs because the absorption signal induced by

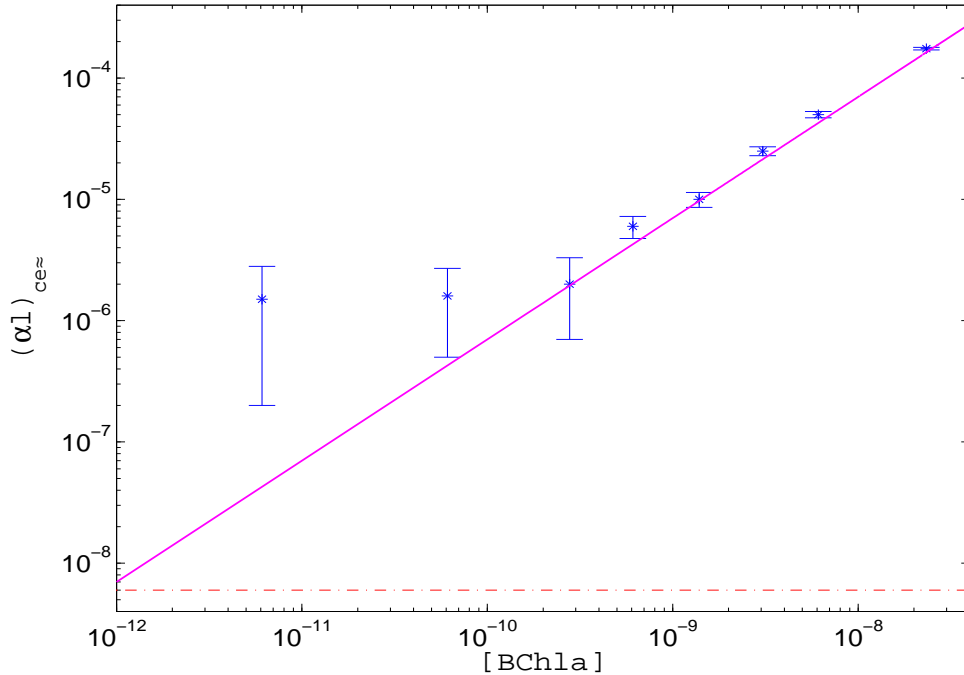


Fig. 2. Cavity-enhanced estimate $(\alpha l)_{ce\approx}$ versus nominal BChla concentration (see text).

very low concentrations dips below our technical noise floor for measuring the reflected optical power; at very low concentrations, the apparent absorption inferred from the data via the estimator $(\alpha l)_{ce\approx}$ is dominated by the optical noise and is thus independent of the concentration. The concentration at which the data points begin to deviate from linear behavior thus indicates the detection threshold of our device, and is seen to be ~ 200 pM. The corresponding sensitivity gain relative to single-pass measurements, from Eq. (17), is $G_{op} \approx 2.3 \times 10^4 \approx 2F_-/\pi$.

5. Discussion

The shot-noise limit (dash-dot line in Fig. 2) actually sits below our demonstrated detection threshold by a factor ~ 200 , meaning that much better performance could in principle be obtained in our setup without any changes to the FP cavity itself. With a finesse of 3.4×10^4 and mode-matched optical power of 60 nW, the shot-noise limited absorption detection threshold would be $\sim 2 \times 10^{-10}/\sqrt{\text{Hz}}$. With 1 s integration time this would correspond to ~ 200 BChla molecules in the cavity mode volume (which in our current device is $\sim 10^{-5} \text{ cm}^3$). The best commercially available mirrors achieve $t_1^2 + t_2^2 \approx 10^{-6}$ and $\delta \approx 2.2 \times 10^{-6}$ [17]; assuming these parameters and adding solvent-induced losses of 5×10^{-7} (scaled from our existing device) for a cavity with $l = 10 \mu\text{m}$, we find $P_{ce-} \approx 0.53P_{inc}$ while the circulating power would be $P_{circ} \approx 1.46 \times 10^5 P_{inc}$ [16]. With 1 m radius-of-curvature mirrors the intracavity spot size would be $\approx 1.7 \times 10^{-12} \text{ cm}^2$, so for an intracavity intensity of 10^5 W/cm^2 (which should keep us below saturation [18]) we could have $P_{ce-} \approx 7 \times 10^{-7} \text{ W}$. The shot-noise limited sensitivity would then be $\approx 1.5 \times 10^{-12}/\sqrt{\text{Hz}}$. This would make it possible to monitor the absorption of an individual BChla molecule with $\sim 2 \text{ kHz}$ bandwidth (near the peak extinction coefficient $\approx 7 \times 10^4 \text{ M}^{-1} \text{ cm}^{-1}$ at 770 nm). One potential technical issue with this extrapolation, however, is the question of what photothermal disturbances might arise at this level of circulating power and

finesse; if they turn out to be significant then it could be interesting to investigate high-finesse, liquid-phase cavity-enhanced photothermal spectroscopy [19, 20] as an alternative.

Acknowledgments

We thank Michael Armen for invaluable technical assistance, as well as Dirk Englund, Orkun Aiken and Muhammed Yildirim for contributions to early stages of this work. This research was supported by the National Science Foundation and the W. M. Keck Foundation.